



TECH BRIEFS

NATIONAL AERONAUTICS AND SPACE ADMINISTRATION

-  **Technology Focus**
-  **Electronics/Computers**
-  **Software**
-  **Materials**
-  **Mechanics/Machinery**
-  **Manufacturing**
-  **Bio-Medical**
-  **Physical Sciences**
-  **Information Sciences**
-  **Books and Reports**

INTRODUCTION

Tech Briefs are short announcements of innovations originating from research and development activities of the National Aeronautics and Space Administration. They emphasize information considered likely to be transferable across industrial, regional, or disciplinary lines and are issued to encourage commercial application.

Availability of NASA Tech Briefs and TSPs

Requests for individual Tech Briefs or for Technical Support Packages (TSPs) announced herein should be addressed to

National Technology Transfer Center

Telephone No. (800) 678-6882 or via World Wide Web at www.nttc.edu

Please reference the control numbers appearing at the end of each Tech Brief. Information on NASA's Innovative Partnerships Program (IPP), its documents, and services is also available at the same facility or on the World Wide Web at <http://www.nasa.gov/offices/ipp/network/index.html>

Innovative Partnerships Offices are located at NASA field centers to provide technology-transfer access to industrial users. Inquiries can be made by contacting NASA field centers listed below.

NASA Field Centers and Program Offices

Ames Research Center

Lisa L. Lockyer
(650) 604-1754
lisa.l.lockyer@nasa.gov

Dryden Flight Research Center

Gregory Poteat
(661) 276-3872
greg.poteat@dfrc.nasa.gov

Glenn Research Center

Kathy Needham
(216) 433-2802
kathleen.k.needham@nasa.gov

Goddard Space Flight Center

Nona Cheeks
(301) 286-5810
nona.k.cheeks@nasa.gov

Jet Propulsion Laboratory

Andrew Gray
(818) 354-3821
gray@jpl.nasa.gov

Johnson Space Center

information
(281) 483-3809
jsc.techtran@mail.nasa.gov

Kennedy Space Center

David R. Makufka
(321) 867-6227
david.r.makufka@nasa.gov

Langley Research Center

Brian Beaton
(757) 864-2192
brian.f.beaton@nasa.gov

Marshall Space Flight Center

Jim Dowdy
(256) 544-7604
jim.dowdy@msfc.nasa.gov

Stennis Space Center

Ramona Travis
(228) 688-3832
ramona.e.travis@nasa.gov

Carl Ray, Program Executive

Small Business Innovation
Research (SBIR) & Small
Business Technology
Transfer (STTR) Programs
(202) 358-4652
carl.g.ray@nasa.gov

Doug Comstock, Director

Innovative Partnerships
Program Office
(202) 358-2560
doug.comstock@nasa.gov



TECH BRIEFS

NATIONAL AERONAUTICS AND SPACE ADMINISTRATION



5 Technology Focus: Sensors

- 5 Active and Passive Hybrid Sensor
- 5 Quick-Response Thermal Actuator for Use as a Heat Switch
- 6 System for Hydrogen Sensing
- 6 Method for Detecting Perlite Compaction in Large Cryogenic Tanks
- 7 Using Thin-Film Thermometers as Heaters in Thermal Control Applications
- 7 Directional Spherical Cherenkov Detector
- 8 AlGaN Ultraviolet Detectors for Dual-Band UV Detection



9 Electronics/Computers

- 9 K-Band Traveling-Wave Tube Amplifier
- 9 Simplified Load-Following Control for a Fuel Cell System
- 10 Modified Phasemeter for a Heterodyne Laser Interferometer
- 11 Loosely Coupled GPS-Aided Inertial Navigation System for Range Safety
- 11 Sideband-Separating, Millimeter-Wave Heterodyne Receiver



13 Manufacturing & Prototyping

- 13 Coaxial Propellant Injectors With Faceplate Annulus Control
- 14 Adaptable Diffraction Gratings With Wavefront Transformation



15 Materials

- 15 Optimizing a Laser Process for Making Carbon Nanotubes
- 16 Thermogravimetric Analysis of Single-Wall Carbon Nanotubes



17 Mechanics/Machinery

- 17 Robotic Arm Comprising Two Bending Segments
- 18 Magnetostrictive Brake
- 19 Low-Friction, Low-Profile, High-Moment Two-Axis Joint
- 19 Foil Gas Thrust Bearings for High-Speed Turbomachinery
- 20 Miniature Multi-Axis Mechanism for Hand Controllers



21 Physical Sciences

- 21 Digitally Enhanced Heterodyne Interferometry
- 22 Focusing Light Beams To Improve Atomic-Vapor Optical Buffers



23 Information Sciences

- 23 Landmark Detection in Orbital Images Using Saliency Histograms
- 23 Efficient Bit-to-Symbol Likelihood Mappings
- 24 Capacity Maximizing Constellations



27 Software

- 27 Natural-Language Parser for PBEM
- 27 Policy Process Editor for P³BM Software
- 27 A Quality System Database
- 27 Trajectory Optimization: OTIS 4
- 28 Computer Software Configuration Item-Specific Flight Software Image Transfer Script Generator

This document was prepared under the sponsorship of the National Aeronautics and Space Administration. Neither the United States Government nor any person acting on behalf of the United States Government assumes any liability resulting from the use of the information contained in this document, or warrants that such use will be free from privately owned rights.



Active and Passive Hybrid Sensor

The sensor acquires active and passive measurements to map ocean winds.

Goddard Space Flight Center, Greenbelt, Maryland

A hybrid ocean wind sensor (HOWS) can map ocean vector wind in low to hurricane-level winds, and non-precipitating and precipitating conditions. It can acquire active and passive measurements through a single aperture at two wavelengths, two polarizations, and multiple incidence angles. Its low profile, compact geometry, and low power consumption permits installation on aircraft platforms, including high-altitude unmanned aerial vehicles (UAVs).

The primary innovation enabling both active and passive measurements through a single system, while allowing for beam scanning, is the separation of transmit and receive beam synthesis process. With this approach, the antenna comprises several linear arrays, each with its own transceiver. The key components to this system are the transceiver, antenna, and multi-channel digital receiver subsystems. The antenna design was described in "Low-Profile, Dual-Wavelength, Dual-Polarized Antenna" (GSC-15706), *NASA Tech Briefs*, Vol. 34, No. 1 (January 2010), p. 26.

A novel capability of this design is that each transceiver has an internal calibration loop that is interconnected with adjacent transceivers. This allows the relative phase of the waveform generators and LO (local oscillator) signals to be directly measured. With environmental

changes, the relative phase distribution can change, which potentially degrades the antenna pattern due to phase errors and biases. Direct measurement of the LO phase and transmit phase alleviates this problem.

The system will operate at C and Ku-bands with beams at 30° and 40° incidence. The retrieval processor will use the active and passive measurements to map the ocean vector wind with a pixel resolution of approximately 2x2 km. With a more than 100-MHz bandwidth, it can operate in a high-resolution mode to provide very high-resolution imagery.

The system design operates in two separate modes: transmission and reception. During transmission, the phase and amplitude distribution of the array are controlled through the transceivers. Every n -th transmission cycle, the internal calibration circuits are used to measure the relative phase and amplitude differences introduced by the circuits themselves so that these offsets can be accounted for in forming the transmitted beam pattern. During reception, the receivers amplify and down-convert the receive backscatter and observed scene emission. The digitized signals are sent to the digital receiver subsystem, which applies phase and amplitude weightings to form the desired receive antenna pat-

tern. The receiver circuit also contains a Dicke switch and noise diode circuit to implement Dicke-Hach mode receiver. The bandwidth of the antenna and receiver paths is large enough that the passive signal is filtered from the active signal so that both may be measured simultaneously.

HOWS is useful for monitoring surface winds during severe ocean storms. Search and rescue missions can benefit from both the imaging capabilities of this system as well as the retrieved products. Although this system is focused on ocean vector winds, its ability to collect dual-wavelength, dual-polarized active and passive measurements and image over a range of incidence angles in a conically scanning or fixed pointing mode has broad use for remote sensing and surveillance purposes. Potential uses other than wind applications include mapping land, snow, and ice features. Its capabilities also can aid in target or scene classification, as well as high-resolution imaging from airborne or ground surveillance applications.

This work was done by James R. Carswell of Remote Sensing Solutions, Inc. for Goddard Space Flight Center. Further information is contained in a TSP (see page 1). GSC-15707-1

Quick-Response Thermal Actuator for Use as a Heat Switch

Thermal actuators have many applications in aerospace, automotive, and energy storage.

NASA's Jet Propulsion Laboratory, Pasadena, California

This work improves the performance of a heat switch, or a thermal actuator, by delivering heat to the actuator in a more efficient manner. The method uses a heat pipe as the plunger or plug instead of just using a solid piece of metal. The heat pipe could be one tailored for fast transient thermal response.

A heat switch/thermal actuator works by using the expansion of a paraf-

fin wax as it melts as a means of moving a piston/plug/plunger to perform a function. Typically, this function is to close a small gap and increase heat transfer across a boundary, but it also could be used to move a latch. These devices are usually slow, and the stroke of the piston/plunger is very small.

A device of this kind could replace the need for heat switches that require power to operate on a spacecraft in a safe-mode

condition. This device would require no power to operate except for the waste heat of the device it is protecting. It may also be used as an energy-harvesting device by using waste heat to move a piston back and forth much faster than could be accomplished otherwise.

The device uses waste heat that flows through the plunger pedestal into the heat pipe and out towards the paraffin wax to cause actuation of the plunger

due to phase change of the wax from solid to liquid. For use as a heat switch on a spacecraft, multiple devices may be permanently attached to a radiator via the plunger, and the body attached to a rigid structure. During a safe mode orbital maneuver if the radiator should face the Sun, the device will then push off the radiator, disengaging it from the spacecraft bus. The device could be mounted as a pull device as well, pulling the radiator closer to the thermal bus to

increase the thermal conductance between bus and radiator.

Thermal actuators of this kind are somewhat common, except that this device uses a heat pipe as a plunger, so this is an improvement. Most other devices require heat transfer through the wax chamber body, not through the plunger itself. This device will have three distinct advantages over other versions:

- Fast actuation due to quick heat transfer.
- Large stroke and stroke velocity.

- Mass savings as there is no need for thick metallic sections for conducting heat.

The actuation stroke could be designed to be large and quick enough to be used as an energy-harvesting device, converting waste heat into mechanical energy.

This work was done by Juan Cepeda-Rizo of Caltech for NASA's Jet Propulsion Laboratory. Further information is contained in a TSP (see page 1). NPO-46679

System for Hydrogen Sensing

John H. Glenn Research Center, Cleveland, Ohio

A low-power, wireless gas-sensing system is designed to safeguard the apparatus to which it is attached, as well as associated personnel. It also ensures the efficiency and operational integrity of the hydrogen-powered apparatus. This sensing system can be operated with lower power consumption (less than 30 nanowatts), but still has a fast response. The detecting signal can be wirelessly transmitted to remote locations, or can be posted on the Web. This system can also be operated by harvesting energy.

The electrical signal response of the sensor to the hydrogen gas can be amplified by a differential detection interface (DDI) connected to the low-power gas sensor. A microcontroller is connected and programmed to process the electrical signal, which is then wirelessly transmitted. The system also includes a central monitoring station with a wireless receiver configured to receive the sensor data signal from the wireless transmitter of the sensor device. The system further includes a power source with at least one

vibrational energy harvester, solar energy harvester, and a battery.

This work was done by Jenshan Lin, David P. Norton, Stephen J. Pearton, and Fan Ren of the University of Florida for Glenn Research Center. Further information is contained in a TSP (see page 1).

Inquiries concerning rights for the commercial use of this invention should be addressed to NASA Glenn Research Center, Innovative Partnerships Office, Attn: Steve Fedor, Mail Stop 4-8, 21000 Brookpark Road, Cleveland, Ohio 44135. Refer to LEW-18484-1.

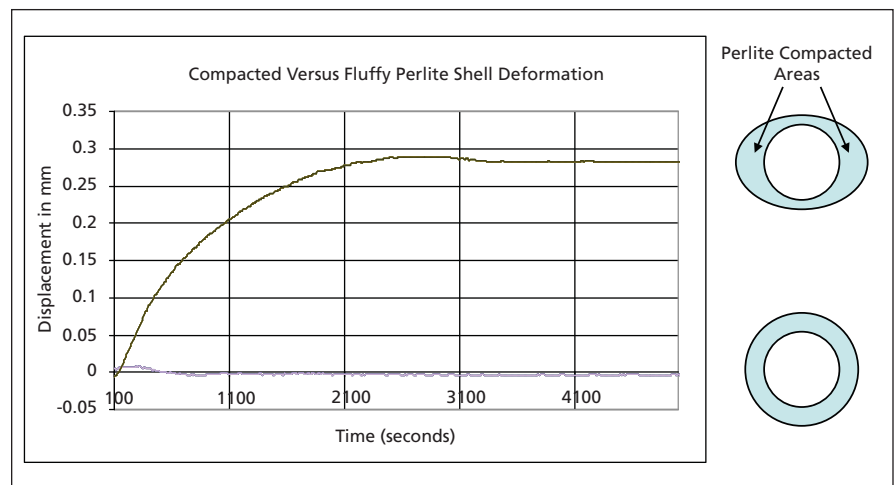
Method for Detecting Perlite Compaction in Large Cryogenic Tanks

This technique could be applied by companies using rail cars and trucks to deliver liquid cryogenics.

John F. Kennedy Space Center, Florida

Perlite is the most typical insulating powder used to separate the inner and outer shells of cryogenic tanks. The inner tank holds the low-temperature commodity, while the outer shell is exposed to the ambient temperature. Perlite minimizes radiative energy transfer between the two tanks. Being a powder, perlite will settle over time, leading to the danger of transferring any loads from the inner shell to the outer shell. This can cause deformation of the outer shell, leading to damaged internal fittings.

The method proposed is to place strain or displacement sensors on several locations of the outer shell. Loads induced on the shell by the expanding inner shell and perlite would be monitored, providing an indication of the location and degree of compaction.



Strain/Displacement Measurements for the detection of perlite compaction. The curves show the differential motion of the outer tank as the inner tank thermally expanded with fluffy perlite (lower curve) and compacted perlite (upper curve).

Testing involved a small, metal Dewar tank composed of an inner and outer shell. The annular region was filled with perlite. Displacement sensors were connected at two locations on the outside of the outer shell. With the perlite not compacted, the inner tank was thermally cycled and the difference in the two displacements was measured as the inner tank warmed and pressed on the perlite.

The perlite was then compacted by hand in two areas while the inner tank was cold in order to mechanically couple the inner and outer shells. When the inner tank was allowed to warm and expand, it deformed the outer tank into an elliptical shape, and the displacement sensors detected different motions for the fluffy and compacted perlite. In any location where the perlite was still fluffy and not compacted, there was no defor-

mation. In areas where the perlite was packed more solidly, the sensors detected a slight deflection. By running these checks between cycles, it becomes a simple matter to identify areas of perlite compaction, and replace it before it can cause damage to the outer shell.

This work was done by Robert Youngquist of Kennedy Space Center. Further information is contained in a TSP (see page 1). KSC-13214

Using Thin-Film Thermometers as Heaters in Thermal Control Applications

NASA's Jet Propulsion Laboratory, Pasadena, California

A cryogenic sensor maintains calibration at ≈ 4.2 K to better than 2 mK (<0.5 percent resistance repeatability) after being heated to ≈ 40 K with ≈ 0.5 W power. The sensor withstands 4 W power dissipation when immersed in liquid nitrogen with verified resistance reproducibility of, at worst, 1 percent. The

sensor maintains calibration to 0.1 percent after being heated with 1-W power at ≈ 77 K for a period of 48 hours.

When operated with a readout scheme that is capable of mitigating the self-heating calibration errors, this and similar sensors can be used for precision (mK stability) temperature control with-

out the need of separate heaters and associated wiring/cabling.

This work was done by Hyung J. Cho, Konstantin Penanen, Kalyani G. Sukhatme, and Warren A. Holmes of Caltech, and Scott Courts of Lake Shore Cryotronics for NASA's Jet Propulsion Laboratory. Further information is contained in a TSP (see page 1). NPO-46882

Directional Spherical Cherenkov Detector

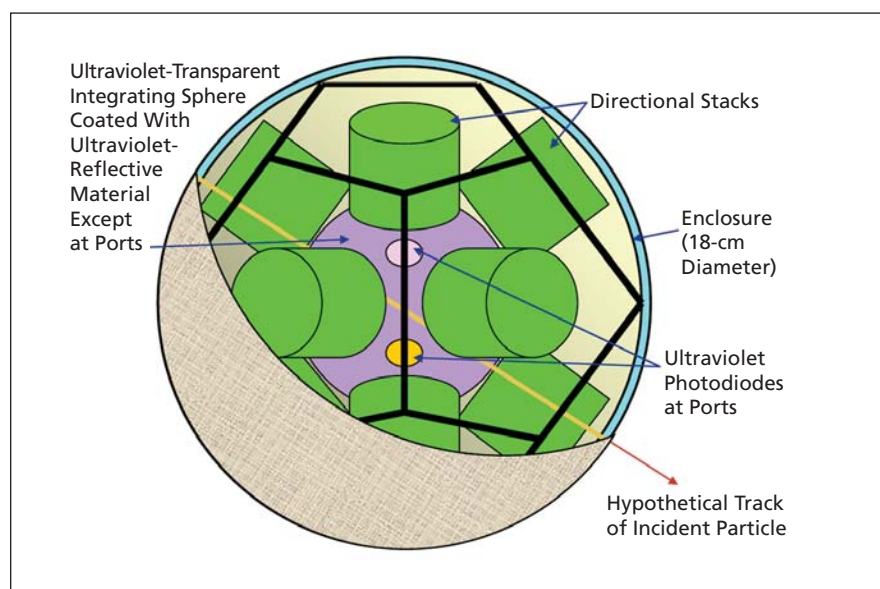
Incident particles could be sorted by direction, speed, and electric charge.

John H. Glenn Research Center, Cleveland, Ohio

A proposed radiation-detecting apparatus would provide information on the kinetic energies, directions, and electric charges of highly energetic incident subatomic particles. The apparatus was originally intended for use in measuring properties of cosmic rays in outer space, but could also be adapted to terrestrial uses — for example, radiation dosimetry aboard high-altitude aircraft and in proton radiation therapy for treatment of tumors.

The apparatus (see figure) would include a spherical Cherenkov detector surrounded by stacks of pairs of detectors. Each such pair and stack would be used in identifying incident particles and would respond to particles incident within a solid-angle range that, in conjunction with the number of such stacks, would define the angular resolution of the apparatus. The number of stacks and the number of pairs of detectors in each stack may be unlimited.

The detectors in each stack would typically have areas >1 cm² and could be made, variously, from compensated sili-



A Spherical Cherenkov Detector would be combined with directional/triggering detector stacks.

con or from such wide-bandgap semiconductors as semi-insulating silicon carbide. Sheets of tungsten, lead, nickel, iron, and/or alloys thereof, serving as

energy-moderating materials, could be inserted between detectors to enable discrimination of particles by energy. A scintillation counter could be used as a

particle trigger with, or in place of, the detector stack.

The spherical Cherenkov detector would include a sphere of ultraviolet-transparent material (e.g., sapphire, quartz, or an acrylic polymer) having an ultraviolet index of refraction greater than 1. The sphere would be coated with an ultraviolet-reflecting material except at small ports. SiC photodiodes or optical fibers leading to photodiodes would be mounted facing into the sphere at the ports to enable detection of Cherenkov ultraviolet light emitted within the sphere.

The detectors in the stacks would serve as triggers for collection of light by the photodiodes of the spherical

Cherenkov counter. The direction and length of the path of a triggering particle would be determined from the identities (and thus the positions) of the affected detectors and stacks. For incident ions having sufficiently high kinetic energies, the strengths of the signals from the SiC photodiodes or optical fibers would be proportional to the square of the electric charges of the ions multiplied by the path lengths. Hence, a velocity distribution for high-energy ions incident from multiple directions could be determined.

For less-energetic incident particles, further sorting could be accomplished through correlation of the Cherenkov signal from the sphere with differences

among signals from stacked detectors that have different thicknesses and that may be interspersed with energy-moderating materials. Sensitivity of detection could be increased through substitution of low-noise SiC detectors for ordinary SiC detectors.

This work was done by John D. Wrbanek, Gustave C. Fralick, and Susan Y. Wrbanek of Glenn Research Center. Further information is contained in a TSP (see page 1).

Inquiries concerning rights for the commercial use of this invention should be addressed to NASA Glenn Research Center, Innovative Partnerships Office, Attn: Steve Fedor, Mail Stop 4-8, 21000 Brookpark Road, Cleveland, Ohio 44135. Refer to LEW-18362-1.

AlGa_xN Ultraviolet Detectors for Dual-Band UV Detection

This technology can be used in multicolor imaging for flame temperature sensing and counter-camouflage/biosensing applications.

Goddard Space Flight Center, Greenbelt, Maryland

This innovation comprises technology that has the ability to measure at least two ultraviolet (UV) bands using one detector without relying on any external optical filters. This allows users to build a miniature UVA and UVB monitor, as well as to develop compact, multicolor imaging technologies for flame temperature sensing, air-quality control, and terrestrial/counter-camouflage/biosensing applications.

The structure is designed for back illumination and contains six AlGa_xN layers with different doping, Al percentage, and two contacts — A and B. The cut-off wavelength of AlGa_xN can be tuned from 200 nm to 365 nm by changing the Al percentage. There are three band-edges in this structure that correspond to Al_xGa_{1-x}N, Al_yGa_{1-y}N, and Al_zGa_{1-z}N — x , y , and z should be designed to be $x > y > z$ for back illumination.

When photons are injected from the backside, they will be absorbed at differ-

ent layers depending on the wavelength of the photons. Electrically, the device is a back-to-back pin structure along the vertical direction. When B is biased positively, and A is connected to the ground, the bottom pin is forwardly biased and acts as a current variable resistor with resistance becoming negligible when the bias on B is high enough. While the bottom pin is forward biased, the top pin junction is reverse biased and acts as a detector. Because the depletion mainly happens in the n-Al_zGa_{1-z}N layer, only the photons absorbed in n-Al_zGa_{1-z}N will be converted into photon-current. When the bias is applied in an opposite manner, in which B is biased negatively and A is connected to the ground, the bottom pin is biased in reverse and acts as an active detector. The depletion region is mainly in n-Al_yGa_{1-y}N and the photons with $wx < wp < wy$ can be converted into photocurrent. When $wp < wx$, all photons will

be absorbed in the bottom n-Al_xGa_{1-x}N layer. Most of the photoelectrons will be recombined locally without generating photocurrent.

By changing the polarity of the bias, the detector can selectively detect two different wavebands: $wy < wp < wz$, when positive bias is applied on A, and $wx < wp < wy$ when negative bias is applied on A. The detector is blind to $wp < wx$ (no photocurrent) and $wp > wz$ (no absorption). Practically, wx , wy , and wz are tunable between 250 nm to 300 nm. The percentage of Al in the p+ layer in the center can be any number between y and z . As a result, the two detection bands do not have to be continuous.

This work was done by Laddawan Miko, David Franz, and Carl M. Stahle of Goddard Space Flight Center and Feng Yan and Bing Guan of MEI Technologies, Inc. Further information is contained in a TSP (see page 1). GSC-15163-1



K-Band Traveling-Wave Tube Amplifier

This amplifier can be used for high-data-rate transmission from communications satellites.

John H. Glenn Research Center, Cleveland, Ohio

A new space-qualified, high-power, high-efficiency, K-band traveling-wave tube amplifier (TWTA), shown in the figure, will provide high-rate, high-capacity, direct-to-Earth communications for science data and video gathered by the Lunar Reconnaissance Orbiter (LRO) during its mission. The TWTA is designed for 20 years of operational life, well in excess of the expected 7 years of mission life. It is a vacuum electronics device that is used to amplify microwave communications signals. TWTs are needed for high-frequency and high-power applications, such as communications from the Moon, because they have significantly higher power capability and efficiency than solid-state devices. Amplification in a TWT is by a factor of about 100,000. The RF power and data rate values for the LRO TWTA, when compared with other space based K-band transmitters, are an order of magnitude higher and represent a new state of the art.

Several technological advances were responsible for the successful demonstration of the K-band TWTA. A numerical model enabled manufacturing a wide-band TWT with high power output and efficiency leading to a first-pass design success. A dual-anode isolated-focus electrode electron gun enabled excellent focusing, which kept the power loss due to beam interception minimal over a wide range of voltage and current values. A WR-34 waveguide was used for the input/output couplers and larger,



A K-Band 40-W TWTA is shown here for the Lunar Reconnaissance Orbiter Mission.

thicker RF quartz windows, allowing operation not only at LRO frequencies but also at future near-Earth mission frequencies. Furthermore, it is more robust against mechanical shock and vibrations, and lowers the total attenuation of the signal in the waveguide run between the TWT output and the antenna. An external filter was developed to suppress the unwanted conducted emissions from the EPC (electronic power conditioner) to the spacecraft bus by greater than 20 dB.

The TWTA has successfully completed a vigorous spaceflight qualification effort, including random vibration testing and cycling between temperature extremes

that the hardware is expected to experience during mission operation. Other possible applications include high-data-rate transmission from geosynchronous communications satellites to Earth.

This work was done by Dale A. Force, Rainee N. Simons, and Todd T. Peterson of Glenn Research Center, and Paul C. Spitsen of L-3 Communications Electron Technologies, Inc. Further information is contained in a TSP (see page 1).

Inquiries concerning rights for the commercial use of this invention should be addressed to NASA Glenn Research Center, Innovative Partnerships Office, Attn: Steve Fedor, Mail Stop 4-8, 21000 Brookpark Road, Cleveland, Ohio 44135. Refer to LEW-18443-1.

Simplified Load-Following Control for a Fuel Cell System

A load-dependent voltage would be used to control a parasitic device.

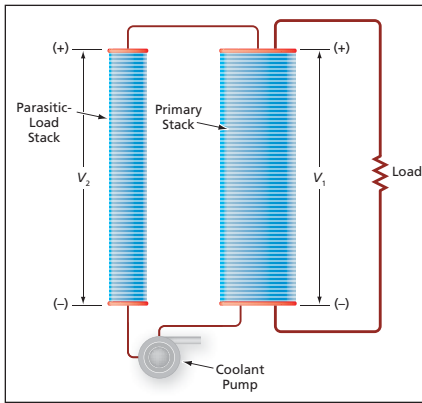
Lyndon B. Johnson Space Center, Houston, Texas

A simplified load-following control scheme has been proposed for a fuel cell power system. The scheme could be used to control devices that are important parts of a fuel cell system but are sometimes characterized as parasitic because they consume some of the power

generated by the fuel cells.

The parasitic devices can include the following: a pump for circulating coolant to remove waste heat, pumps for circulating reactant gases and humidifying inlet gases, an electric heater for keeping the fuel cell stack

above a minimum operating temperature when the production of waste heat is insufficient for this purpose, and a centrifugal water separator. Operating these parasitic devices steadily at their full power levels would waste power, reducing the overall efficiency



The Voltage Applied to the Coolant Pump ($V_2 - V_1$) would increase as V_1 decreased with increasing current through the load.

of the fuel cell power system. In general, the power demands for optimal operation of the parasitic devices vary with the load (e.g., the optimum coolant-circulation power increases with the load). The power levels of the parasitic devices in fuel cell power systems can be regulated at optimal levels by electronic feedback control systems that include sensors (e.g., current, voltage, temperature, or

motor-speed sensors) and power-conditioning subsystems. However, such control systems can sometimes be so complex as to detract from the overall reliability of the affected fuel cell power systems.

In the proposed scheme, a single approximate control signal, generated by relatively simple means, would be used for controlling one or more parasitic devices. The scheme is based on the fact that the terminal voltage of a fuel cell stack decreases with increasing current (in other words, voltage decreases with increasing load) even more strongly than does the voltage of a typical battery having a nominally equivalent current and voltage rating. The figure depicts a simple fuel cell system in which the scheme would be applied to control of a coolant pump. The system would include a primary fuel cell stack and a lower-power secondary fuel cell stack denoted the parasitic-load stack. The two fuel cell stacks would be electrically connected at their positive ends. The coolant pump would be connected between the negative ends of the two stacks.

An increase in the power demand of the load would cause a decrease in the voltage of the primary stack, thereby causing an increase in $V_2 - V_1$, the difference between the voltages of the parasitic-load and primary stacks. This, in turn, would cause an increase in the power supplied to the coolant pump. In a design process, that would entail careful selection of the stack cell areas, the numbers of cells in the two stacks, the electrical resistance of the coolant pump, and other design parameters; it should be possible to make the power supplied to the coolant pump, as a function of the load level, closely approximate the amount required for dissipation of waste heat at that level.

This work was done by Arturo Vasquez of Johnson Space Center. Further information is contained in a TSP (see page 1).

This invention is owned by NASA, and a patent application has been filed. Inquiries concerning nonexclusive or exclusive license for its commercial development should be addressed to the Patent Counsel, Johnson Space Center, (281) 483-0837. Refer to MSC-24169-1.

Modified Phasemeter for a Heterodyne Laser Interferometer

An FPGA-based design could be exported to other heterodyne laser interferometers.

NASA's Jet Propulsion Laboratory, Pasadena, California

Modifications have been made in the design of instruments of the type described in "Digital Averaging Phasemeter for Heterodyne Interferometry" (NPO-30866), *NASA Tech Briefs*, Vol. 28, No. 9 (September 2004), page 6a. To recapitulate: A phasemeter of this type measures the difference between the phases of the unknown and reference heterodyne signals in a heterodyne laser interferometer. This phasemeter performs well enough to enable interferometric measurements of displacements with accuracy of the order of 100 pm. This is a single, integral system capable of performing three major functions that, heretofore, have been performed by separate systems: (1) measurement of the fractional-cycle phase difference, (2) counting of multiple cycles of phase change, and (3) averaging of phase measurements over multiple cycles for improved resolution. This phasemeter also offers the advantage of making repeated measurements at a high rate: the phase is measured on every heterodyne

cycle. Thus, for example, in measuring the relative phase of two signals having a heterodyne frequency of 10 kHz, the phasemeter would accumulate 10,000 measurements per second. At this high measurement rate, an accurate average phase determination can be made more quickly than is possible at a lower rate.

At the time of writing the cited prior article, the phasemeter design lacked immunity to drift of the heterodyne frequency, was bandwidth-limited by computer bus architectures then in use, and was resolution-limited by the nature of field-programmable gate arrays (FPGAs) then available. The modifications have overcome these limitations and have afforded additional improvements in accuracy, speed, and modularity.

The modifications are summarized as follows:

- Taking advantage of improvements made in FPGAs since the original design effort, major phasemeter functions are implemented in a commercial, off-the-shelf FPGA card. It is

necessary to add supplementary interface electronic circuitry to support legacy peripheral equipment, but even so, it is significantly easier to implement the phasemeter in the modified design than in the original high-speed-digital-board design.

- In the previous design, a reference clock signal having a frequency of 128 MHz was generated outside the FPGA and delivered to the FPGA board via a coaxial cable. Since many commercial FPGAs contain built-in phase-locked-loop frequency multipliers, it has become feasible to utilize these multipliers to internally generate a reference clock signal in response to a precise externally generated reference signal having a frequency between 10 and 20 MHz. In addition, the internally generated reference clock signal has a higher frequency — 200 MHz — and, hence, affords higher resolution.
- Modularity is enhanced by incorporation of a microprocessor-type peripheral

eral component interface (PCI) block, making the phasemeter design exportable to a variety of computer architectures. The PCI interface can transfer an entire block of phasemeter registers at a rate of 10 kHz.

- A few hardware components were added to enable measurement of the

heterodyne-signal period, to count reference clock cycles during an averaging cycle, and to utilize the resulting data in such a way as to make the phasemeter immune to drift of the heterodyne frequency. These additions also eliminate the necessity of incorporating, into the phaseme-

ter software, a different reference-clock-cycle parameter for every different heterodyne frequency that might be used.

This work was done by Frank M. Loya of Caltech for NASA's Jet Propulsion Laboratory. Further information is contained in a TSP (see page 1). NPO-45484

Loosely Coupled GPS-Aided Inertial Navigation System for Range Safety

Goddard Space Flight Center, Greenbelt, Maryland

The Autonomous Flight Safety System (AFSS) aims to replace the human element of range safety operations, as well as reduce reliance on expensive, down-range assets for launches of expendable launch vehicles (ELVs). The system consists of multiple navigation sensors and flight computers that provide a highly reliable platform. It is designed to ensure that single-event failures in a flight computer or sensor will not bring down the whole system. The flight computer uses a rules-based structure derived from range safety requirements to make decisions whether or not to destroy the rocket.

By combining the inertial navigation system (INS) with Global Positioning

System (GPS), the GPS signal can be used to check error growth of the INS and, due to the small, short-term errors of the INS, the system is more accurate than the sensor alone. The fused system helps to solve the common cause failures, and also provides the benefit of graceful degradation of system performance should a failure occur.

This innovation has algorithms developed specifically with range safety applications in mind. The INS and Kalman filter algorithms, including the linearized error model, for integrating the two systems were developed and simulated to determine their performance. The system calculates the errors in the

IMU and provides information on the quality of the data it outputs to aid the AFSS system in determining what level of trust to give the data.

The filter is designed in such a way that there is always position and velocity output. Loss of GPS will not cause the INS to go unstable, or to cease information output. Also, covariance estimates and the error states are available to the user for further use in determining data quality.

This work was done by Scott Heatwole and Raymond J. Lanzi for Goddard Space Flight Center. For further information, contact the Goddard Innovative Partnerships Office at (301) 286-5810. GSC-15549-1

Sideband-Separating, Millimeter-Wave Heterodyne Receiver

NASA's Jet Propulsion Laboratory, Pasadena, California

Researchers have demonstrated a sub-millimeter-wave spectrometer that combines extremely broad bandwidth with extremely high sensitivity and spectral resolution to enable future spacecraft to measure the composition of the Earth's troposphere in three dimensions many times per day at spatial resolutions as high as a few kilometers. Microwave limb sounding is a proven remote-sensing technique that measures thermal emission spectra from molecular gases along limb views of the Earth's atmosphere against a cold space background.

The new receiver will down-convert thermal emission spectra in the 180–300

GHz band using superconductor-insulator-superconductor (SIS) heterodyne mixers. A technique called sideband separation is used to provide 24 GHz of instantaneous bandwidth from a single receiver, enabling many chemical species to be measured simultaneously by a single receiver with accurate calibration. The high sensitivity provided by SIS mixers will enable accurate measurements of chemicals at low concentrations with very short integration times. A novel scanning telescope, also under development at the Jet Propulsion Laboratory, will take advantage of these short integration times to measure

three-dimensional maps of the concentration of a large number of key chemical species in the troposphere over nearly the entire planet five to nine times per day. These frequent measurements will enable researchers to both monitor air quality and to understand how pollution is transported by the atmosphere.

This work was done by John S. Ward, Bruce Bumble, Karen A. Lee, Jonathan H. Kawamura, Goutam Chattopadhyay, Paul Stek, and Frank Rice of Caltech for NASA's Jet Propulsion Laboratory. Further information is contained in a TSP (see page 1). NPO-46205



Coaxial Propellant Injectors With Faceplate Annulus Control

These injectors are simpler and less expensive, relative to prior coaxial injectors.

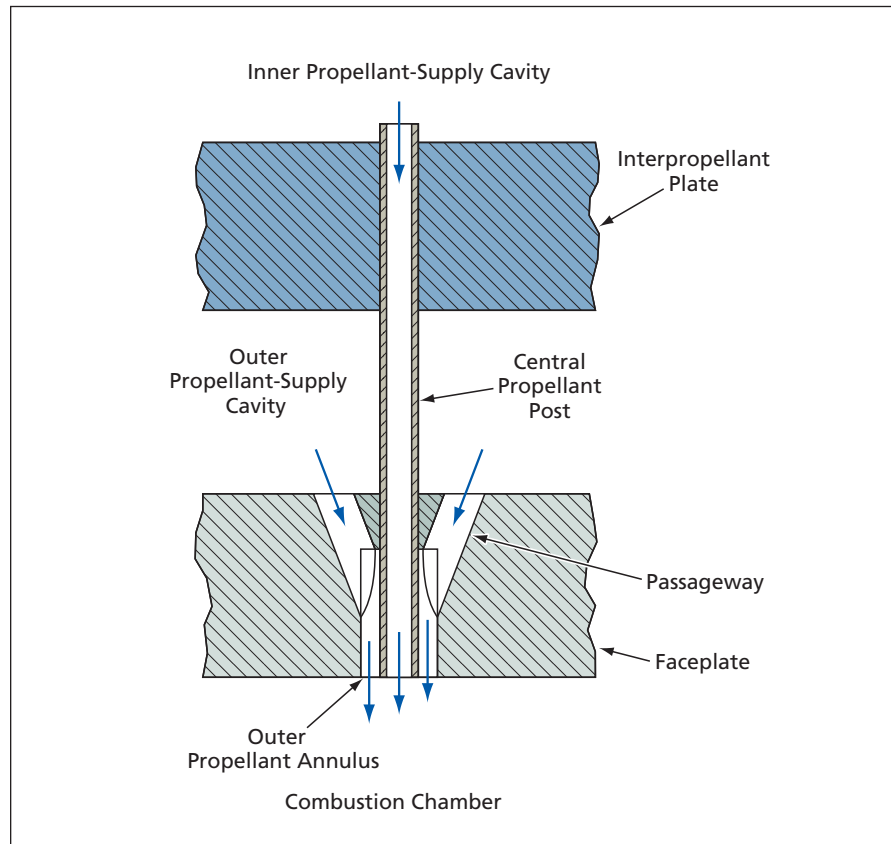
Marshall Space Flight Center, Alabama

An improved design concept for coaxial propellant injectors for a rocket engine (or perhaps for a non-rocket combustion chamber) offers advantages of greater robustness, less complexity, fewer parts, lower cost, and less bulk, relative to prior injectors of equivalent functionality. This design concept is particularly well suited to small, tight-tolerance injectors, for which prior designs are not suitable because the practical implementation of those designs entails very high costs and difficulty in adhering to the tolerances.

The concept applies to a system for simultaneous injection of two propellant fluids — one (typically, an oxidizer) stored in an inner propellant-supply cavity and the other (typically, a fuel) stored in an outer propellant-supply cavity. The two propellant supply cavities are separated by an interpropellant plate, and the outer propellant-supply cavity is separated from the combustion chamber by a faceplate.

The figure presents a simplified cross-sectional view of a coaxial injector according to this concept. The injector includes a central propellant post, which is a tube that extends from the inner propellant-supply cavity, through the faceplate, ending at a location flush with the combustion-chamber surface of the faceplate. An annulus for forming an annular flow outer propellant surrounding the central flow of inner propellant and features for maintaining the lateral alignment of the central propellant post relative to this annular flow are integral parts of the faceplate, machined from the faceplate, as described below. First, a through hole that defines the minor diameter of the annulus and that holds the central propellant post in lateral alignment relative to the annulus is drilled into the faceplate. Next, the outer diameter of the annulus is formed as a precise counterbore to the through hole.

By means of electrical-discharge machining or another method suited to the specific design, slanted passageways are formed to allow flow from the outer propellant cavity to the annulus. The number and dimensions of these passages depend on the specific design and are chosen to



The **Outer Propellant Annulus**, passageways for the outer propellant, and associated features for maintaining the coaxial alignment of the central propellant tube are machined into the faceplate.

ensure uniform annular exit flow.

The central propellant post can be fabricated from drawn, centerless-ground tubing. One end of the central propellant post is bonded to the interpropellant plate, completing a seal that maintains separation between the two propellants prior to injection. The other end of the central propellant post can float freely in the through hole, or, for additional support, it can be bonded to the faceplate at either or both end(s) of the through hole.

In the combustion chamber, the jet of inner propellant flowing from the outer end of the central propellant post mixes with the annular flow of outer propellant, and the resulting mixture burns. The physical and chemical properties of the propellants and the injection geom-

etry are major determinants of the efficiency of the combustion process.

This work was done by Mark D. Horn of The Boeing Co., Shinjiro Miyata, and Shahram Farhangi formerly of The Boeing Co. for Marshall Space Flight Center.

Title to this invention has been waived under the provisions of the National Aeronautics and Space Act (42 U.S.C. 2457(f)) to The Boeing Company. Inquiries concerning licenses for its commercial development should be addressed to:

*Patent Administration
The Boeing Company
15460 Laguna Canyon Road
MC 1650-7006
Irvine, CA 92618*

Refer to MFS-32306-1, volume and number of this NASA Tech Briefs issue, and the page number.

Adaptable Diffraction Gratings With Wavefront Transformation

Better resolution and aberration control are possible with a dynamic refractive grating.

Goddard Space Flight Center, Greenbelt, Maryland

Diffraction gratings are optical components with regular patterns of grooves, which angularly disperse incoming light by wavelength. Traditional diffraction gratings have static planar, concave, or convex surfaces. However, if they could be made so that they can change the surface curvature at will, then they would be able to focus on particular segments, self-calibrate, or perform fine adjustments.

This innovation creates a diffraction grating on a deformable surface. This surface could be bent at will, resulting in a dynamic wavefront transformation. This allows for self-calibration, compensation for aberrations, enhancing image resolution in a particular area, or performing multiple scans using different wavelengths. A dynamic grating gives scientists a new ability to explore wavefronts from a variety of viewpoints.

To create these gratings, surface relief diffraction grating grooves are formed

on a flat substrate. Flat substrate is technologically the most convenient option for any type of gratings ruling and is especially essential for lithographically scribed gratings. Lithographic scribing is the newly developed method first commercially introduced by Light-Smyth, which produces gratings with the highest performance and arbitrary groove shape/spacing for advanced aberration control. Next, an imprint of the grating is made on a deformable substrate, such as thin polymer film. The imprinted deformable substrate is then stretched over a circular, oval, or otherwise shaped opening, much like a membrane on a drumhead. The opening is connected with a chamber with the inside pressure that may be controlled by the user. The exact curvature of the substrate depends on the elasticity of the membrane, the difference between air or gas pressures on two sides of the substrate, and the shape of the opening. Very complex and challenging

surface profiles may be obtained with relatively simple and inexpensive shaping of the opening. For example, oval opening produces generally toroidal grating surface.

Pressure is applied to one side of the substrate in order to change its curvature. As the curvature changes, so does the wavefront transformation of the diffracted (or reflected) light. Such wavefront transformations can be used to optimize imaging or spectra in a particular diffraction order, or imaging of reflected light. The ability to do so in a single unit is a major advance in the state of the art. Even without the dynamic aspect, this method provides a unique way of creating complex grating surface profiles for advanced optical designs using simple mechanical means.

This work was done by Dmitri Iazikov, Thomas W. Mossberg, and Christoph M. Greiner of Goddard Space Flight Center. Further information is contained in a TSP (see page 1). GSC-15679-1



Optimizing a Laser Process for Making Carbon Nanotubes

Trends in process parameters for optimization and scale-up have been identified.

Lyndon B. Johnson Space Center, Houston, Texas

A systematic experimental study has been performed to determine the effects of each of the operating conditions in a double-pulse laser ablation process that is used to produce single-wall carbon nanotubes (SWCNTs). The comprehensive data compiled in this study have been analyzed to recommend conditions for optimizing the process and scaling up the process for mass production.

The double-pulse laser ablation process for making SWCNTs was developed by Rice University researchers. Of all currently known nanotube-synthesizing processes (arc and chemical vapor deposition), this process yields the greatest proportion of SWCNTs in the product material. In the normal version of this process, one uses a green (wavelength 532 nm) laser pulse followed by an infrared (wavelength 1,064 nm) laser pulse within a few nanoseconds to ablate a metal-containing graphite target located in a flow of argon at 100 standard cubic centimeters per minute (sccm) at

a pressure of 500 torr (≈ 66.7 kPa) in a flow tube that is maintained in an oven at a temperature of 1,473 K. The aforementioned process conditions are important for optimizing the production of SWCNTs and scaling up production. Reports of previous research (mostly at Rice University) toward optimization of process conditions mention effects of oven temperature and briefly mention effects of flow conditions, but no systematic, comprehensive study of the effects of process conditions was done prior to the study described here.

This was a parametric study, in which several production runs were carried out, changing one operating condition for each run. The study involved variation of a total of nine parameters: the sequence of the laser pulses, pulse-separation time, laser pulse energy density, buffer gas (helium or nitrogen instead of argon), oven temperature, pressure, flow speed, inner diameter of the flow tube, and flow-tube material. The same graphite target was used in all the runs.

The nanotube-containing material produced in each run was collected and characterized by a variety of analytical techniques.

The results of the characterizations indicated trends in the effects of process parameters that could be used to optimize the process and increase the efficiency of the production process. Among the conclusions (see table) reached in this study is that SWCNT material of better quality can be produced by use of lower pressure and faster flow, relative to the normal version of the process. This conclusion could be useful in scaling up the process. This limited study could be extended by changing more than one parameter at a time in an effort to identify some of the intricate mutual effects of different process parameters.

This work was done by Sivaram Arepalli, Pavel Nikolaev, and William Holmes of GB Tech Inc. for Johnson Space Center. Further information is contained in a TSP (see page 1). MSC-23508-1

| Parameter | Normal Condition | Conclusions |
|------------------------|-----------------------|--|
| Temperature | 1,473 K (1,200 °C) | Lower temperature gives narrower, weaker tubes. |
| Laser Energy Density | 1.5 J/cm ² | Higher energy density produces C60 and narrower tubes that may contain less metal. |
| Pulse Sequence | Green Before Infrared | Green should be first. Green repeated (no infrared) is better. |
| Pulse Separation | 50 nanoseconds | Slightly longer delay may be helpful. |
| Buffer Gas | Argon | Don't use helium. Nitrogen is probably acceptable. |
| Pressure | 66.7 kPa (500 torr) | Lower pressure is preferable. |
| Flow Rate | 100 sccm | Higher flow rate is better. |
| Diameter of Inner Tube | 2.5 cm | Narrower is bad. |
| Inner Tube Material | Quartz | Alumina is better. |

Some Conclusions concerning nine process parameters were reached in a parametric study.

Thermogravimetric Analysis of Single-Wall Carbon Nanotubes

An improved protocol yields greater consistency.

Lyndon B. Johnson Space Center, Houston, Texas

An improved protocol for thermogravimetric analysis (TGA) of samples of single-wall carbon nanotube (SWCNT) material has been developed to increase the degree of consistency among results so that meaningful comparisons can be made among different samples. This improved TGA protocol is suitable for incorporation into the protocol for characterization of carbon nanotube material as described in the preceding article.

TGA has been used extensively to characterize carbon nanotube materials during the past decade. In most cases, TGA of carbon nanotube materials is performed in gas mixtures that contain oxygen at various concentrations. The data acquired in TGA following this approach provide information on ash content and on oxidation temperature (which is usually described as the temperature of the maximum rate of loss of weight). In many cases, rates of loss of weight have several maxima at temperatures ranging from 300 to 800 °C. These peaks have been attributed to various components in the nanotube material, including amorphous carbon, nanotubes, and graphitic particles.

Metal particles are always present in nanotube materials because the metals

are used as catalysts in the production of the nanotubes. The position of each oxidation peak is strongly affected by the amounts and microstructures of the metal particles because these particles also catalyze oxidation of all carbon forms present in the nanotube material.

The ash content is used to determine the amount of metal catalyst in the material. It is usually assumed that upon completion of TGA, all carbon has been removed in the forms of CO and CO₂ and that all remaining material consists of metal oxides.

It has been observed that different TGA results can be obtained from the same nanotube material on different TGA apparatuses and even in different runs on the same apparatus. These inconsistencies can be attributed to the use of a wide variety of sample-preparation practices, instruments, protocols, heating rates, and carrier gases and to inhomogeneities within nanotube batches. In the improved TGA protocol, knowledge gained in a study of the effects of TGA experimental parameters on TGA results is applied to reduce the inconsistencies substantially. In all of the experiments in the study, air was used as the gas mixture and the flow rate was 100 standard cubic centimeters per minute.

The improved protocol is summarized as follows:

1. Use a heating rate of 5 °C/min up to the maximum temperature. The exact value of maximum temperature can be varied; 800 °C accommodates most samples.
2. The mass of the sample should be between 2 and 4 mg.
3. Three separate TGA runs should be performed on each sample.
4. In addition to the TGA weight measurement, an independent weight measurement should be performed on a microbalance, after TGA, to increase the precision of determination of the ash content.
5. Results from the three runs should be processed to obtain the mean values of oxidation temperature(s) and ash content.
6. Results from the three runs should also be processed to obtain standard deviations of the oxidation temperature(s) and ash content. These standard deviations are representative of inhomogeneity in the sample.

This work was done by Sivaram Arepalli, Pavel Nikolaev, and Olga Gorelik of GB Tech Inc. for Johnson Space Center. Further information is contained in a TSP (see page 1). MSC-23507-1.



Robotic Arm Comprising Two Bending Segments

Thinness and multiple bending contribute to dexterity for operation in hitherto inaccessible places.

Lyndon B. Johnson Space Center, Houston, Texas

The figure shows several aspects of an experimental robotic manipulator that includes a housing from which protrudes a tendril- or tentacle-like arm 1 cm thick and 1 m long. The arm con-

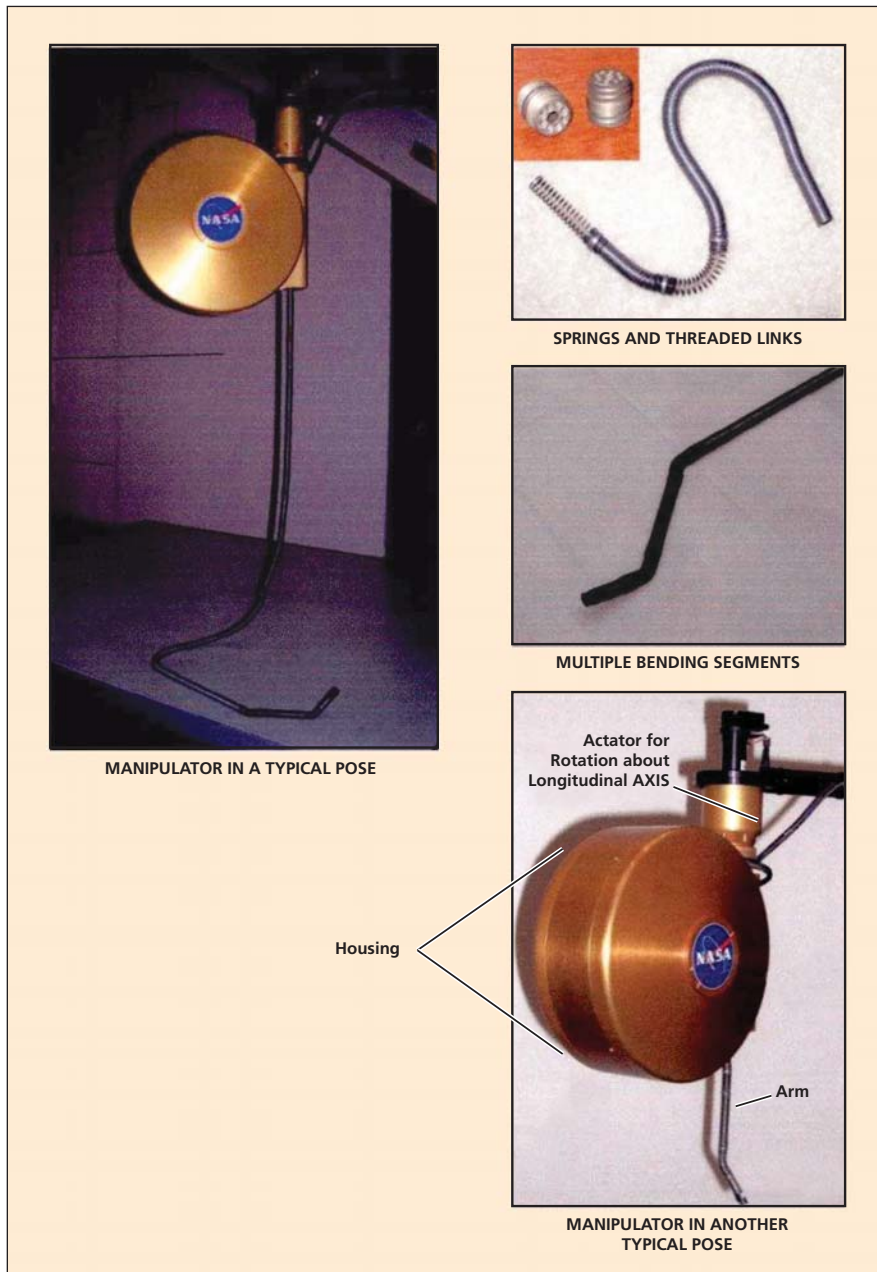
sists of two collinear segments, each of which can be bent independently of the other, and the two segments can be bent simultaneously in different planes. The arm can be retracted to a mini-

mum length or extended by any desired amount up to its full length. The arm can also be made to rotate about its own longitudinal axis.

Some prior experimental robotic manipulators include single-segment bendable arms. Those arms are thicker and shorter than the present one. The present robotic manipulator serves as a prototype of future manipulators that, by virtue of the slenderness and multiple-bending capability of their arms, are expected to have sufficient dexterity for operation within spaces that would otherwise be inaccessible. Such manipulators could be especially well suited as means of minimally invasive inspection during construction and maintenance activities.

Each of the two collinear bending arm segments is further subdivided into a series of collinear extension- and compression-type helical springs joined by threaded links. The extension springs occupy the majority of the length of the arm and engage passively in bending. The compression springs are used for actively controlled bending. Bending is effected by means of pairs of antagonistic tendons in the form of spectra gel spun polymer lines that are attached at specific threaded links and run the entire length of the arm inside the spring helix from the attachment links to motor-driven pulleys inside the housing. Two pairs of tendons, mounted in orthogonal planes that intersect along the longitudinal axis, are used to effect bending of each segment. The tendons for actuating the distal bending segment are in planes offset by an angle of 45° from those of the proximal bending segment: This configuration makes it possible to accommodate all eight tendons at the same diameter along the arm.

The threaded links have central bores through which power and video wires can be strung (1) from a charge-coupled-device camera mounted on the tip of the arms (2) back along the interior of the arm into the housing and then (3) from within the housing to an exter-



The Arm Extends From the Housing, which can be mounted on an actuator to effect rotation around the longitudinal axis of the arm. The housing has an outside diameter of 23 cm and a length of 13 cm along its cylindrical axis.

nal video monitor. Each link also contains guide holes for the tendons at equal angular intervals around the longitudinal axis.

The housing contains electronic control circuitry and the motors, pulleys, and other actuator mechanisms for effecting extension, retraction, and bending. For extension and retraction, the arm is wound on a motor-driven reel inside the housing. A spiral groove on the circumference of the reel guides the arm during extension or retraction and confines the arm to a single layer during multiple revolutions, so that a complex reeling mechanism is not necessary to prevent binding. The arm extends from

the reel out of the housing along a salient tube that is tangential to the reel. The salient tube also extends tangentially in the direction opposite that of the arm. This tube extension can be attached to a stationary fixture if rotation about the longitudinal axis is not desired. Alternatively, this tube extension can be attached to the output shaft of a stationary motor drive that can be used to effect rotation of the housing about the longitudinal axis of the tube, thereby effecting rotation of the arm about its longitudinal axis.

The system for controlling the pose of the arms is a standard position-control system based on a proportional + inte-

gral control loop, except as follows: the loop includes a washout filter (which is a special high-pass filter that, among other things, passes transient inputs while suppressing steady-state inputs) to take advantage of the inherent hysteretic friction of the tendon drive. The washout filter makes it possible to maintain a desired position by means of a small motor command aided by the inherent friction.

This work was done by Joshua S. Mehling, Myron A. Diffler, and Robert O. Ambrose of Johnson Space Center; Mars W. Chu of Metrica, Inc.; and Michael C. Valvo of Jacobs Sverdrup. Further information is contained in a TSP (see page 1). MSC-24128-1

⚙️ Magnetostrictive Brake

Power demand would be reduced by 75 percent.

Lyndon B. Johnson Space Center, Houston, Texas

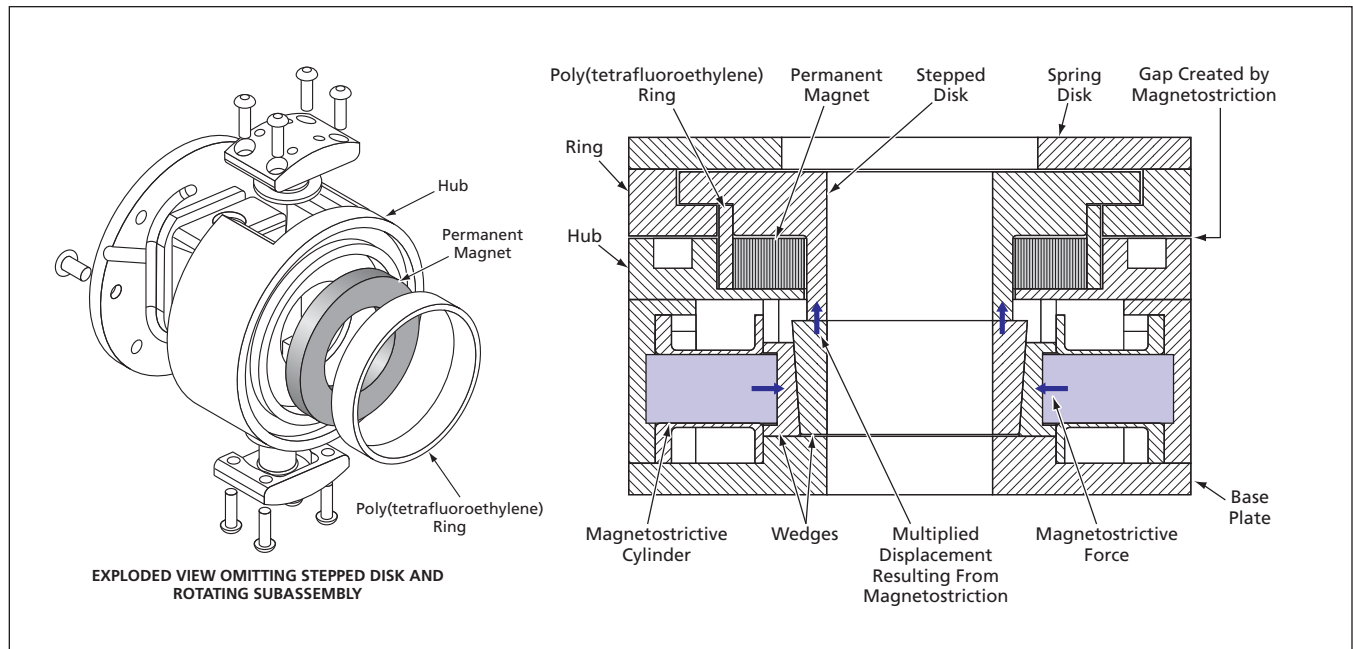
A magnetostrictive brake has been designed as a more energy-efficient alternative to a magnetic fail-safe brake in a robot. (In the specific application, “fail-safe” signifies that the brake is normally engaged; that is, power must be supplied to allow free rotation.) The magnetic fail-safe brake must be supplied with about 8 W of electric power to initiate and maintain disengagement. In contrast, the magnetostrictive brake, which would have about the same dimensions and the

same torque rating as those of the magnetic fail-safe brake, would demand only about 2 W of power for disengagement.

The brake (see figure) would include a stationary base plate and a hub mounted on the base plate. Two solenoid assemblies would be mounted in diametrically opposed recesses in the hub. The cores of the solenoids would be made of the magnetostrictive alloy Terfenol-D or equivalent. The rotating part of the brake would be a ring-and-

spring-disk subassembly. By means of leaf springs not shown in the figure, this subassembly would be coupled with the shaft that the brake is meant to restrain.

With no power supplied to the solenoids, a permanent magnet would pull axially on a stepped disk and on a shelf in the hub, causing the ring to be squeezed axially between the stepped disk and the hub. The friction associated with this axial squeeze would effect the braking action.



In the **Magnetostrictive Brake**, a large braking force would be generated by the permanent magnet. When power was supplied to electromagnet coils (not shown) surrounding the magnetostrictive cylinders in the solenoid assemblies, the resulting magnetostrictive strain would be converted to a force and displacement that would oppose the braking force.

Supplying electric power to the solenoids would cause the magnetostrictive cylinders to push radially inward against a set of wedges that would be in axial contact with the stepped disk. The wedges would convert the radial magnetostrictive strain to a multiplied

axial displacement of the stepped disk. This axial displacement would be just large enough to lift the stepped disk, against the permanent magnetic force, out of contact with the ring. The ring would then be free to turn because it would no longer be

squeezed axially between the stepped disk and the hub.

This work was done by Myron A. Diftler and Aaron Hulse of Lockheed Martin Corp. for Johnson Space Center. Further information is contained in a TSP (see page 1), MSC-23629-1

Low-Friction, Low-Profile, High-Moment Two-Axis Joint

This device can be utilized in robotics, automobile steering, transmission systems, and aircraft control surface linkages.

Lyndon B. Johnson Space Center, Houston, Texas

The two-axis joint is a mechanical device that provides two-degrees-of-freedom motion between connected components. A compact, moment-resistant, two-axis joint is used to connect an electromechanical actuator to its driven structural members. Due to the requirements of the overall mechanism, the joint has a low profile to fit within the allowable space, low friction, and high moment-reacting capability. The mechanical arrangement of this joint can withstand high moments when loads are applied. These features allow the joint to be used in tight spaces where a high load capability is required, as well as in applications where penetrating the mounting surface is not an option or where surface mounting is required.

The joint consists of one base, one clevis, one cap, two needle bearings, and a circular shim. The base of the joint is the housing (the base and the cap together), and is connected to the grounding structure via fasteners and a bolt pattern. Captive within the housing, between the base and the cap, are the rotating clevis and the needle bearings.

The clevis is attached to the mechanical system (linear actuator) via a pin. This pin, and the rotational movement of the clevis with respect to the housing, provides two rotational degrees of freedom.

The larger diameter flange of the clevis is sandwiched between a pair of needle bearings, one on each side of the flange. During the assembly of the two-axis joint, the circular shims are used to adjust the amount of preload that is applied to the needle bearings. The above arrangement enables the joint to handle high moments with minimal friction.

To achieve the high-moment capability within a low-profile joint, the use of "depth of engagement" (like that of a conventional rotating shaft) to react moment is replaced with planar engagement parallel to the mounting surface. The needle bearings with the clevis flange provide the surface area to react the clevis loads/moments into the joint housing while providing minimal friction during rotation. The diameter of the flange and the bearings can be increased to react higher loads and still maintain a compact surface mounting capability.

This type of joint can be used in a wide variety of mechanisms and mechanical systems. It is especially effective where precise, smooth, continuous motion is required. For example, the joint can be used at the end of a linear actuator that is required to extend and rotate simultaneously. The current design application is for use in a spacecraft docking-system capture mechanism. Other applications might include industrial robotic or assembly line apparatuses, positioning systems, or in the motion-based simulator industry that employs complex, multi-axis manipulators for various types of motions.

This work was done by James L. Lewis of Johnson Space Center and Thang Le and Monty B. Carroll of Lockheed Martin. Further information is contained in a TSP (see page 1).

This invention is owned by NASA, and a patent application has been filed. Inquiries concerning nonexclusive or exclusive license for its commercial development should be addressed to the Patent Counsel, Johnson Space Center, (281) 483-1003. Refer to MSC-23881-1.

Foil Gas Thrust Bearings for High-Speed Turbomachinery

John H. Glenn Research Center, Cleveland, Ohio

A methodology has been developed for the design and construction of simple foil thrust bearings intended for parametric performance testing and low marginal costs, supporting continued development of oil-free turbomachinery. A bearing backing plate is first machined and surface-ground to produce flat and parallel faces. Partial-arc slots needed to retain the foil components are then machined into the plate by wire

electrical discharge machining. Slot thicknesses achievable by a single wire pass are appropriate to accommodate the practical range of foil thicknesses, leaving a small clearance in this hinged joint to permit limited motion. The backing plate is constructed from a nickel-based superalloy (Inconel 718) to allow heat treatment of the entire assembled bearing, as well as to permit high-temperature operation. However, other

dimensionally stable materials, such as precipitation-hardened stainless steel, can also be used for this component depending on application.

The top and bump foil blanks are cut from stacks of annealed Inconel X-750 foil by the same EDM process. The bump foil has several azimuthal slits separating it into five individual bump strips. This configuration allows for variable bump spacing, which helps to ac-

commodate the effects of the varying surface velocity, thermal crowning, centrifugal dishing, and misalignment. Rectangular tabs on the foil blanks fit into the backing plate slots.

For this application, a rather traditional set of conventionally machined dies is selected, and bump foil blanks are pressed into the dies for forming. This

arrangement produces a set of bump foil dies for foil thrust bearings that provide for relatively inexpensive fabrication of various bump configurations, and employing methods and features from the public domain.

This work was done by Brian Edmonds and Christopher DellaCorte of Glenn Research Center and Brian Dykas of Case Western Reserve

University. Further information is contained in a TSP (see page 1).

Inquiries concerning rights for the commercial use of this invention should be addressed to NASA Glenn Research Center, Innovative Partnerships Office, Attn: Steve Fedor, Mail Stop 4-8, 21000 Brookpark Road, Cleveland, Ohio 44135. Refer to LEW-18397-1.

Miniature Multi-Axis Mechanism for Hand Controllers

Lyndon B. Johnson Space Center, Houston, Texas

A hand controller provides up to three axes of motion, and all required feel characteristics (stiffness and breakout torques) located inside a hollow handle within the grip of the hand. This is achieved using a miniature gimbal mechanism that allows for independent motion about one, two, or three axes within the grip volume of the hand, and miniature flexure assemblies co-located with the gimbal mechanism that provide substantial stiffness and breakout torques in each axis of motion. Also, miniature sensors can be integrated into the gimbal mechanism, also located

within the grip volume of the hand, to provide direct angular position measurement for each axis of motion.

Previous designs either had the pivot axes located outside the grip envelope, or used mechanical linkages to couple the axes of motion to remotely located spring mechanisms and sensors. This proposed design is not susceptible to vibration, shock, or g-loading in any axis, is of the smallest possible size and weight, and is highly reliable.

This work was done by Pablo Bandera and Paul Buchele of Honeywell, Inc. for Johnson Space Center. For further information, contact

the JSC Innovation Partnerships Office at (281) 483-3809.

Title to this invention has been waived under the provisions of the National Aeronautics and Space Act {42 U.S.C. 2457(f)} to Honeywell, Inc. Inquiries concerning licenses for its commercial development should be addressed to:

Honeywell, Inc.

P.O. Box 52199

Phoenix, AZ 85072

Refer to MSC-24457-1, volume and number of this NASA Tech Briefs issue, and the page number.



Digitally Enhanced Heterodyne Interferometry

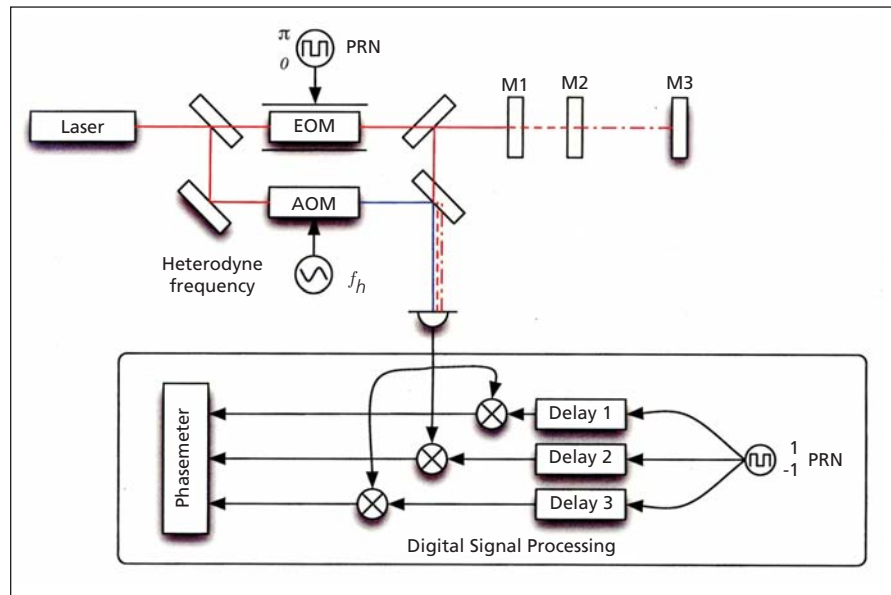
This design mitigates cyclic error and improves measurement sensitivity.

NASA's Jet Propulsion Laboratory, Pasadena, California

Spurious interference limits the performance of many interferometric measurements. Digitally enhanced interferometry (DEI) improves measurement sensitivity by augmenting conventional heterodyne interferometry with pseudo-random noise (PRN) code phase modulation. DEI effectively changes the measurement problem from one of hardware (optics, electronics), which may deteriorate over time, to one of software (modulation, digital signal processing), which does not. DEI isolates interferometric signals based on their delay. Interferometric signals are effectively time-tagged by phase-modulating the laser source with a PRN code. DEI improves measurement sensitivity by exploiting the autocorrelation properties of the PRN to isolate only the signal of interest and reject spurious interference. The properties of the PRN code determine the degree of isolation.

Heterodyne interferometers are used for metrology to measure the distance to a remote mirror, usually with several intermediate surfaces for steering and beam-shaping. These surfaces, while necessary, can degrade the measurement. A digitally enhanced heterodyne interferometer makes the same measurement, with the primary difference being the addition of an electro-optic modulator that adds zero or π phase shift onto the measurement beam before it goes out to the measurement surface. The electronics system has an additional front end that demodulates the PRN code before the phase measurement (see figure).

The PRN code used is a maximal-length sequence. This sequence has the property that, when correlated with itself, is one and, when correlated with a delayed version of itself, the correlation can be as low as $1/N$, where N is the length of the code sequence (chip length). The pseudo-random code appears as white noise on the photodetector. The heterodyne signal appears only after the signal is demodulated with the proper delay by the electronics. Cyclic



A Digitally Enhanced Heterodyne measurement system includes an electro-optic modulator (EOM) and an additional front end on the phasemeter that demodulates the PRN code before the phase is measured for the metrology.

errors can be suppressed up to $1/N$ by adjusting the delay of the PRN code in the front end of the phasemeter to measure the desired signal and reject spurious interference. By adjusting the delay properly, signals from the spurious reflections can also be analyzed.

PRN code modulation is conceptually similar to code division multiplexing, which is used in communications for spread spectrum signals. The technology for this is widespread and mature. PRN codes are commonly used in metrology, e.g. lidar systems, by amplitude modulating a laser with a PRN code and performing range measurements based on the code. The sensitivity of these measurements is determined by the characteristic wavelength of the PRN code. In contrast, digitally enhanced interferometry sensitivity is determined by the optical wavelength, not the code, and is several orders of magnitude more sensitive.

Another benefit of delay-based signal isolation is the ability to measure multiple optical components with a single metrology system. This multiplexing capability

significantly simplifies measurements of multiple components, such as displacement monitoring of a train of optics or segments of a multi-mirror telescope. This design's immunity to scattered light and electronic interference will allow measurements to approach the fundamental limits of shot noise and electronic noise, allowing for laboratory-class performance in real-world environments.

This work was done by Daniel Shaddock, Brent Ware, Oliver Lay, and Serge Dubovitsky of Caltech for NASA's Jet Propulsion Laboratory.

In accordance with Public Law 96-517, the contractor has elected to retain title to this invention. Inquiries concerning rights for its commercial use should be addressed to:

*Innovative Technology Assets Management
JPL*

*Mail Stop 202-233
4800 Oak Grove Drive
Pasadena, CA 91109-8099*

E-mail: iaoffice@jpl.nasa.gov

Refer to NPO-45188, volume and number of this NASA Tech Briefs issue, and the page number.

🌀 Focusing Light Beams To Improve Atomic-Vapor Optical Buffers

Atomic-vapor optical buffers could be made to perform more nearly optimally.

NASA's Jet Propulsion Laboratory, Pasadena, California

Specially designed focusing of light beams has been proposed as a means of improving the performances of optical buffers based on cells containing hot atomic vapors (e.g., rubidium vapor). There is also a companion proposal to improve performance by use of incoherent optical pumping under suitable conditions.

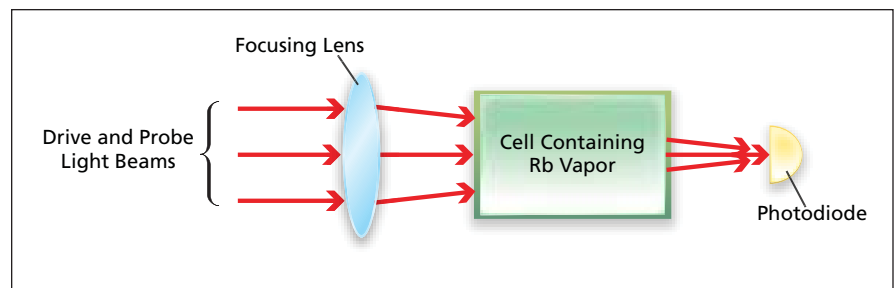
Atomic-vapor optical buffers (of which there are both cold- and hot-vapor types) are photonic devices based on a "slow light" phenomenon that involves quantum effects that occur in vapors of rubidium and other elements under suitable conditions. Atomic-vapor optical buffers have been extensively discussed in the literature as means of optical storage and optical processing of information.

Regarding the proposal to use focusing: The utility of atomic-vapor optical buffers as optical storage and processing devices has been severely limited by nonuniform spatial distributions of intensity in optical beams, arising from absorption of the beams as they propagate in atomic-vapor cells. Such nonuniformity makes it impossible to optimize the physical conditions throughout a cell, thereby making it impossible to optimize the performance of the cell as an optical buffer. In practical terms simplified for the sake of brevity, "to optimize" as used here means to design the cell so as to maximize the group delay of an optical pulse while keeping the absorption and distortion of the pulse reasonably small.

The basic limit of the group delay in the presence of Raman amplification of a probe light beam in a hot-atomic-vapor cell is set by the absorption of a drive light beam with consequent gradual decrease of the width of an electromagnet-

ically induced transparency (EIT) resonance along the propagation direction. One possible approach to compensation of the absorption, represented by the present proposal, is to focus the light (see figure) in such a way that the net effect of the focusing and absorption is

light systems. However, prior studies of those systems did not quantitatively answer the question of whether the performance of an atomic vapor or other medium that exhibits EIT with Raman gain is superior to that of a medium that exhibits EIT without Raman gain.



Light Would Be Focused into and through a hot vapor of rubidium or other suitable atoms. The focusing lens would be designed to produce a beam profile in which focusing would compensate for absorption to yield constant intensity.

that its intensity does not vary with position in the cell. Theoretically, such compensation should lead to fractional group delays longer than those of similar cells in which collimated light is used. It has also been determined theoretically that focusing by a thin spherical-surface lens describable by the geometric-optics approximation would not suffice; It would likely be necessary to use a thick lens of more complex design based at least partly on wave optics.

Regarding the proposal to use incoherent optical pumping: For reasons too complex to describe here, residual absorption of light is one of the main impediments to achievement of desirably long group delays in hot atomic vapors. The present proposal is directed toward suppressing residual absorption of light. The idea of improving the performance of slow-light optical buffers by use of incoherent pumping overlaps somewhat with the basic idea of Raman-based slow-

It is known from prior research that incoherent optical pumping results in (1) suppression of absorption or even amplification of a probe light beam on the one hand, and in (2) destruction of the atomic coherence and broadening of the EIT resonance on the other hand. Suppression of absorption improves the delay-line performance of an atomic-vapor cell, while the destruction of atomic coherence degrades its performance. These considerations were taken into account in a theoretical study performed in support of the proposal to use incoherent optical pumping. The study yielded equations showing that incoherent pumping increases group delay within certain ranges of design and operational parameters.

This work was done by Dmitry Strekalov, Andrey Matsko, and Anatoliy Savchenkov of Caltech for NASA's Jet Propulsion Laboratory. For more information, contact iaoffice@jpl.nasa.gov. NPO-45118



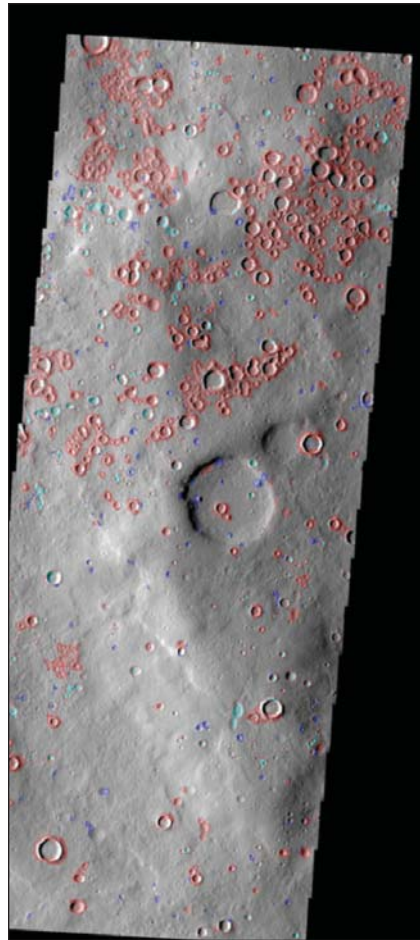
Landmark Detection in Orbital Images Using Saliency Histograms

This technique enables automated identification of objects and regions in airborne or orbital images.

NASA's Jet Propulsion Laboratory, Pasadena, California

NASA's planetary missions have collected, and continue to collect, massive volumes of orbital imagery. The volume is such that it is difficult to manually review all of the data and determine its significance. As a result, images are indexed and searchable by location and date but generally not by their content. A new automated method analyzes images and identifies "landmarks," or visually salient features such as gullies, craters, dust devil tracks, and the like. This technique uses a statistical measure of saliency derived from information theory, so it is not associated with any specific landmark type. It identifies regions that are unusual or that stand out from their surroundings, so the resulting landmarks are context-sensitive areas that can be used to recognize the same area when it is encountered again.

A machine learning classifier is used to identify the type of each discovered landmark. This classifier can also indicate when a previously unknown type of landmark is encountered, enabling the discovery of new and unusual physical phenomena. Using a specified window size, an intensity histogram is computed for each such window within the larger image (sliding the window across the image). Next, a saliency map is computed that specifies, for each pixel, the saliency of the window centered at that pixel. The saliency map is thresholded to identify landmark contours (polygons) using the upper quartile of



Landmarks Are Automatically Identified in THEMIS image V19619013 of Terra Sabaea (Mars). Craters are marked in red, streaks in blue, and unrecognized landmarks in cyan.

saliency values. Descriptive attributes are extracted for each landmark polygon: size, perimeter, mean intensity, standard deviation of intensity, and shape features derived from an ellipse fit. Each landmark is classified as one of a set of known types, or marked as "unknown" using a classifier previously trained on hundreds of manually annotated landmarks. Each image is annotated with its contents (list of landmarks with their locations, types, and attributes).

This method enables fast, automated identification of landmarks to augment or replace manual analysis; fast, automated classification of landmarks to provide semantic annotations; and content-based searches over image archives.

Automated landmark detection in images permits the creation of a summary catalog of all such features in an image database, such as the Planetary Data System (PDS). It could enable entirely new searches for PDS images, based on the desired content (landmark types). In the near future, landmark identification methods using Gabor filters (texture) or covariance descriptors will also be investigated for this application.

This work was done by Kiri L. Wagstaff and Julian Panetta of Caltech; Norbert Schorghofer of the University of Hawaii; and Ronald Greeley, Mary Pendleton Hoffer, and Melissa Bunte of Arizona State University for NASA's Jet Propulsion Laboratory. Further information is contained in a TSP (see page 1). NPO-46674

Efficient Bit-to-Symbol Likelihood Mappings

A new algorithm that increases decoder speed contributes to the development of high-speed optical communications links.

NASA's Jet Propulsion Laboratory, Pasadena, California

This innovation is an efficient algorithm designed to perform bit-to-symbol and symbol-to-bit likelihood mappings that represent a significant portion of the complexity of an error-correction

code decoder for high-order constellations. Recent implementation of the algorithm in hardware has yielded an 8-percent reduction in overall area relative to the prior design. This gain re-

sulted from changing just two operations in a complex decoder. Larger gains are possible for larger constellations that are of interest for deep-space optical communications. The algorithm struc-

tures the bit-to-symbol/symbol-to-bit operations like a tree that forms a portion of a Fast-Fourier-Transform (FFT). Much like an FFT, the parallel computation may be structured in order to reduce repeated computations. Symmetry in the values was noted and allowed for the reduction of the bit-to-symbol mapping by a factor of 2.

This method computes bit-to-symbol likelihood mappings for a soft-in/soft-out decoder that operates over M -ary symbols, but receives and transmits bit-log likelihoods. There are two bit-to-symbol mappings. The first requires $M - 2$ operations and $\log_2 M - 1$ clock cycles. The second requires $O(M \log_2 M)$ operations and $\log_2 \log_2 M$

clock cycles. The symbol-to-bit mapping requires $\log_2 M$ clock cycles and $3M - \log_2 M - 4$ operations. In a pipelined architecture, the reduced operation counts also translate into reduced memory requirement.

This technology can apply to communications channels that use high-order constellations and decode over symbols from that constellation. This would potentially include a large number of communications channels, such as cable modems, disk drives, etc., as well as being a direct improvement to the Optical Communications End-to-End Testbed, which is currently in use to demonstrate, test, and develop deep-space optical communications technology.

This work was done by Bruce E. Moision of Caltech and Michael A. Nakashima of Skillstorm, Incorporated for NASA's Jet Propulsion Laboratory.

In accordance with Public Law 96-517, the contractor has elected to retain title to this invention. Inquiries concerning rights for its commercial use should be addressed to:

*Innovative Technology Assets Management
JPL
Mail Stop 202-233
4800 Oak Grove Drive
Pasadena, CA 91109-8099
E-mail: iaoffice@jpl.nasa.gov
Refer to NPO-44987, volume and number of this NASA Tech Briefs issue, and the page number.*

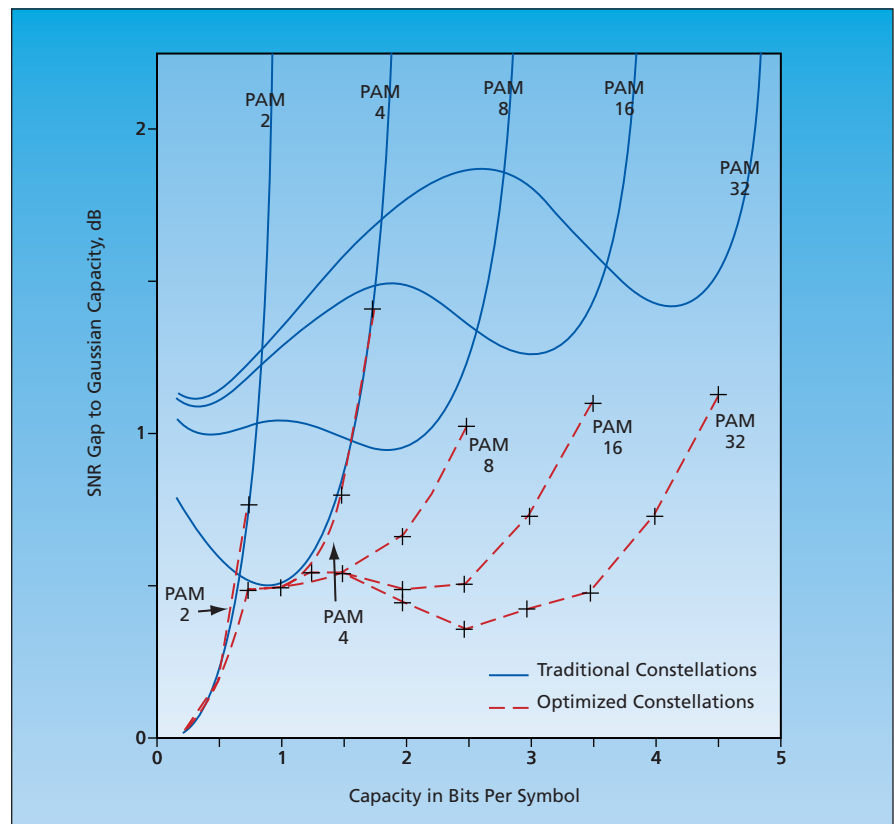
➤ Capacity Maximizing Constellations

Locations and bit labels of constellation points are optimized jointly.

NASA's Jet Propulsion Laboratory, Pasadena, California

Some non-traditional signal constellations have been proposed for transmission of data over the Additive White Gaussian Noise (AWGN) channel using such channel-capacity-approaching codes as low-density parity-check (LDPC) or turbo codes. (As used here, "constellation" signifies, with respect to a signal-modulation scheme, discrete amplitude and/or phase points corresponding to symbols to be transmitted.) Theoretically, in comparison with traditional constellations, these constellations enable the communication systems in which they are used to more closely approach Shannon limits on channel capacities. Computational simulations have shown performance gains of more than 1 dB over traditional constellations. These gains could be translated to bandwidth-efficient communications, variously, over longer distances, using less power, or using smaller antennas.

The opportunity to effect improvements through use of the proposed constellations arises as follows: The introduction of turbo and LDPC codes during the 1990s made it possible to formulate coding schemes that afford near-Shannon-capacity performance for binary and quaternary phase-shift-keying modulation schemes. However, in these and other channel-capacity-approaching coding schemes, when traditional signal constellations are used, the gap between the achievable performance and the Shannon or the Gaussian capacity in-



Gaps Between Parallel Decoding Capacity and Gaussian Capacity [quantified as equivalent signal-to-noise-ratio (SNR) gaps] were computed for optimized and traditional PAM 2-, 4-, 8-, 16-, and 32-point constellations.

creases with bandwidth efficiency (in effect, as more bits are packed into each transmitted symbol). While the channel-capacity-approaching codes are highly

optimized, the traditional signal constellations are not optimized.

The amplitude and/or phase intervals between points in a constellation accord-

ing to the proposal are unequal. Unlike in traditional constellations, both the locations of the points and the bit labels of the points are optimized jointly. In the optimization process, they are chosen to maximize either the joint capacity or the parallel decoding capacity at a target user data rate. Through numerical capacity computations, it has been shown that except in special cases, no constellations are universally optimal for all code rates and that the optimization of a constellation must target a specific code rate.

The proposed constellations have been used in a bit-interleaved coded modulation system employing state-of-the-art LDPC codes. In computational simulations, these constellations were shown to afford performance gains over traditional constellations as predicted by the gap between the parallel decoding capacity of the constellations and the Gaussian capacity (see figure).

This work was done by Maged Barsoum and Christopher Jones of Caltech for NASA's Jet Propulsion Laboratory.

In accordance with Public Law 96-517, the contractor has elected to retain title to this invention. Inquiries concerning rights for its commercial use should be addressed to:

*Innovative Technology Assets Management
JPL*

Mail Stop 202-233

4800 Oak Grove Drive

Pasadena, CA 91109-8099

E-mail: iaoffice@jpl.nasa.gov

Refer to NPO-44810, volume and number of this NASA Tech Briefs issue, and the page number.



➤ Natural-Language Parser for PBEM

A computer program called “Hunter” accepts, as input, a colloquial-English description of a set of policy-based-management rules, and parses that description into a form useable by policy-based enterprise management (PBEM) software.

PBEM is a rules-based approach suitable for automating some management tasks. PBEM simplifies the management of a given enterprise through establishment of policies addressing situations that are likely to occur. PBEM provides a way of managing configurations of network elements, applications, and processes via a set of high-level rules or business policies rather than managing individual elements. Thus, PBEM enables abstraction of the capabilities of the individual elements and switching of control to higher levels.

Development of a system that understands colloquial English is an extremely difficult problem. Because most people do not write perfect English, such a system must be very robust in order to understand what has been written. Hunter is such a system. Recognizing that all possible dialects and variants thereof cannot be anticipated in advance, Hunter was developed to have a unique capability to extract the intended meaning instead of focusing on parsing the exact ways in which individual words are used.

This program was written by Mark James of Caltech for NASA’s Jet Propulsion Laboratory. Further information is contained in a TSP (see page 1).

In accordance with Public Law 96-517, the contractor has elected to retain title to this invention. Inquiries concerning rights for its commercial use should be addressed to:

*Innovative Technology Assets Management
JPL*

Mail Stop 202-233

4800 Oak Grove Drive

Pasadena, CA 91109-8099

E-mail: iaoffice@jpl.nasa.gov

Refer to NPO-45791, volume and number of this NASA Tech Briefs issue, and the page number.

➤ Policy Process Editor for P³BM Software

A computer program enables generation, in the form of graphical representations of process flows with embedded natu-

ral-language policy statements, input to a suite of policy-, process-, and performance-based management (P³BM) software developed at NASA’s Jet Propulsion Laboratory. Like the program described in the immediately preceding article, this program (1) serves as an interface between users and the Hunter software, which translates the input into machine-readable form; and (2) enables users to initialize and monitor the policy-implementation process.

This program provides an intuitive graphical interface for incorporating natural-language policy statements into business-process flow diagrams. Thus, the program enables users who dictate policies to intuitively embed their intended process flows as they state the policies, reducing the likelihood of errors and reducing the time between declaration and execution of policy.

This program was written by Mark James, Hsin-Ping Chang, Edward T. Chow, and Gerald A. Crichton of Caltech for NASA’s Jet Propulsion Laboratory. Further information is contained in a TSP (see page 1).

In accordance with Public Law 96-517, the contractor has elected to retain title to this invention. Inquiries concerning rights for its commercial use should be addressed to:

*Innovative Technology Assets Management
JPL*

Mail Stop 202-233

4800 Oak Grove Drive

Pasadena, CA 91109-8099

E-mail: iaoffice@jpl.nasa.gov

Refer to NPO-45821, volume and number of this NASA Tech Briefs issue, and the page number.

➤ A Quality System Database

A quality system database (QSD), and software to administer the database, were developed to support recording of administrative nonconformance activities that involve requirements for documentation of corrective and/or preventive actions, which can include ISO 9000 internal quality audits and customer complaints. [“ISO 9000” denotes a series of standards, published by the International Organization for Standardization (ISO), for implementation of quality systems to be used in contractual situations.] The software provides for recording and storage of data, enables tracking, and provides status information.

The current version of this QSD software was written in the Microsoft Access

software system and is server-based. Because of an increase in the number of users and the need for data security and reduction in response time, conversion to a Web-based version supported by Oracle software was investigated. As a result, a prototype Web-based version was developed and found to satisfy the aforementioned needs. Efforts are being made to determine the modifications necessary to serve the expanded user base. In addition, the Johnson Space Center ISO auditing group has expressed an interest in adopting this software.

This program was written by William H. Snell, Anne M. Turner, Luther Gifford, and William Stites of United Space Alliance for Johnson Space Center. Further information is contained in a TSP (see page 1). MSC-23447-1

➤ Trajectory Optimization: OTIS 4

The latest release of the Optimal Trajectories by Implicit Simulation (OTIS4) allows users to simulate and optimize aerospace vehicle trajectories. With OTIS4, one can seamlessly generate optimal trajectories and parametric vehicle designs simultaneously. New features also allow OTIS4 to solve non-aerospace continuous time optimal control problems.

The inputs and outputs of OTIS4 have been updated extensively from previous versions. Inputs now make use of object-oriented constructs, including one called a metastring. Metastrings use a greatly improved calculator and common nomenclature to reduce the user’s workload. They allow for more flexibility in specifying vehicle physical models, boundary conditions, and path constraints. The OTIS4 calculator supports common mathematical functions, Boolean operations, and conditional statements. This allows users to define their own variables for use as outputs, constraints, or objective functions.

The user-defined outputs can directly interface with other programs, such as spreadsheets, plotting packages, and visualization programs.

Internally, OTIS4 has more explicit and implicit integration procedures, including high-order collocation methods, the pseudo-spectral method, and several variations of multiple shooting. Users may switch easily between the various methods. Several unique numerical techniques,

such as automated variable scaling and implicit integration grid refinement, support the integration methods.

OTIS4 is also significantly more user friendly than previous versions. The installation process is nearly identical on various platforms, including Microsoft Windows, Apple OS X, and Linux operating systems. Cross-platform scripts also help make the execution of OTIS and post-processing of data easier.

OTIS4 is supplied free by NASA and is subject to ITAR (International Traffic in Arms Regulations) restrictions. Users must have a Fortran compiler, and a Python interpreter is highly recommended.

This work was done by John P. Riehl, Waldy K. Sjauw, and Robert D. Falck of Glenn Research Center and Stephen W. Paris of Boeing Phantom Works. Further information is contained in a TSP (see page 1).

Inquiries concerning rights for the commercial use of this invention should be addressed

to NASA Glenn Research Center, Innovative Partnerships Office, Attn: Steve Fedor, Mail Stop 4-8, 21000 Brookpark Road, Cleveland, Ohio 44135. Refer to LEW-18319-1.

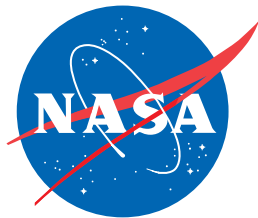
Computer Software Configuration Item-Specific Flight Software Image Transfer Script Generator

A K-shell UNIX script enables the International Space Station (ISS) Flight Control Team (FCT) operators in NASA's Mission Control Center (MCC) in Houston to transfer an entire or partial computer software configuration item (CSCI) from a flight software compact disk (CD) to the onboard Portable Computer System (PCS). The tool is designed to read the content stored on a flight software CD and generate individual CSCI transfer scripts that are capable of transferring the flight software

content in a given subdirectory on the CD to the scratch directory on the PCS. The flight control team can then transfer the flight software from the PCS scratch directory to the Electronically Erasable Programmable Read Only Memory (EEPROM) of an ISS Multiplexer/Demultiplexer (MDM) via the Indirect File Transfer capability.

The individual CSCI scripts and the CSCI Specific Flight Software Image Transfer Script Generator (CFITSG), when executed a second time, will remove all components from their original execution. The tool will identify errors in the transfer process and create logs of the transferred software for the purposes of configuration management.

This work was done by Kenny Bolen and Ronald Greenlaw of The Boeing Company for Johnson Space Center. For further information, contact the JSC Innovation Partnerships Office at (281) 483-3809. MSC-23631-1



National Aeronautics and
Space Administration